CONFERENCE PRE-PRINT

PEELING LIMITED PEDESTALS IN JET-ILW, MAST-U AND TCV: EFFECT OF DENSITY AND ISOTOPE MASS IN DEUTERIUM AND TRITIUM-RICH PLASMA ON PEDESTAL STRUCTURE AND STABILITY AND VALIDATION OF PEDESTAL PREDICTIONS FOR ITER.

L. Frassinetti¹, D. King², S. Saarelma², B. Labit³, S. Blackmore², D. Keeling², C. Perez von Thun⁴, C. Giroud², S. Wiesen⁵, A. Kappatou⁶, N. Vianello⁷, E. Alessi⁸, M. Brix², I.S. Carvalho⁹, P. Carvalho², A. Chomiczewska⁴, J. S. Elmore², M. Fontdecaba¹⁰, E. Giovannozzi¹¹, J. Harrison², S, Hendersson², D. Kos², E. Kowalska⁴, K. Imada¹², M. Lennholm², M. Maslov², A. Meigs², S. Menmuir², R. B. Morales², H. Nyström¹, E. Pawelec¹³, G. Pucella¹¹, R. Scannell², D. Silvagni⁶, A. Stagni⁷, P. Ryan², H.J. Sun², JET Contributors¹⁴, EUROfusion Tokamak Exploitation Team¹⁵, EUROfusion Consortium, JET, Culham Science Centre, Abingdon, OX14 3DB, UK, the MAST Upgrade Team¹⁶, the TCV Team¹⁷.

¹Division of Electromagnetic Engineering and Fusion Science, KTH Royal Institute of Technology, Stockholm SE, ²UKAEA (United Kingdom Atomic Energy Authority), Culham Campus, Abingdon, Oxfordshire, OX14 3DB, UK, ³Ecole Polytechnique Fédérale de Lausanne (EPFL), Swiss Plasma Center (SPC), Lausanne, Switzerland, ⁴Institute of Plasma Physics and Laser Microfusion (IPPLM), Hery 23, 01-497 Warsaw, Poland. ⁵DIFFER - Dutch Institute for Fundamental Energy Research, 5612 AJ Eindhoven, The Netherlands, ⁶Max-Planck-Institut für Plasma Physik, Boltzmannstr.2, 85748 Garching, Germany, ⁷Consorzio RFX, Corso Stati Uniti 4, 35127 Padova, Italy, ⁸Institute for Plasma Science and Technology, CNR, 20125 Milano, Italy, ⁹ITER Organization, Route de Vinon-sur-Verdon, CS 90 046, 13067 St Paul Lez Durance Cedex, France, ¹⁰Laboratorio Nacional de Fusión, CIEMAT, Madrid, Spain, ¹¹Fusion and Nuclear Safety Department - ENEA C. R. Frascati - Frascati (Roma), Italy, ¹² York Plasma Institute, Department of Physics, University of York, YO10 5DD, United Kingdom ¹³Institute of Physics, University of Opole, Poland, ¹⁴See the author list of CF. Maggi et al., Nucl. Fusion 2024, 10.1088/1741-4326/ad3e16, ¹⁵see the author list of E. Joffrin Nuclear Fusion 2024 10.1088/1741-4326/ad2be4 ¹⁶ see author list of J.R. Harrison et al 2019 Nucl. Fusion **59** 112011. ¹⁷See author list of B.P. Duval et al 2024 Nucl. Fusion 64 112023.

Abstract

Plasmas with low collisionality and with the pedestal limited by peeling modes have been achieved in JET-ILW, MAST-U and TCV. The achieved electron-electron pedestal collisionality and the achieved ratio between electron separatrix density to pedestal density are in the ranges $v_e^{*ped} = 0.1 - 0.4$ and $n_e^{sep}/n_e^{ped} = 0.3 - 0.9$, approaching ITER values. In these conditions, the experimental results show that the pedestal pressure increases with increasing density and no degradation of the pedestal pressure with increasing n_e^{sep}/n_e^{ped} has been observed. These behaviours are opposite to what observed in ballooning limited pedestals. However, in all the three machines, both the increase of the pedestal density and the increase of the separatrix density destabilize the ballooning modes and tend to move the pedestal from being peeling limited to being limited by coupled peeling –ballooning modes. The increase of the isotope mass in JET-ILW from deuterium to tritium-rich plasmas leads to an increase of the pedestal pressure, via the increased n_e^{ped} . The Europed pedestal predictions have been validated against the experimental results in all the three machines, showing a reasonable qualitative agreement. The Europed predictions have been applied to ITER showing that the instabilities that will limit its pedestal strongly depend on the values of n_e^{ped} and n_e^{sep} . Nonetheless, assuming type I ELMy H-modes, the ITER pedestal in the Q=10 scenario will reach $p_e^{ped} \approx 60kPa$, with a pedestal pressure that will increase with increasing density and with no degradation at high n_e^{sep}/n_e^{ped} .

1. INTRODUCTION

Modelling and predictive simulations suggest that ITER will operate with pedestal temperature $T^{ped} \approx 4 - 5keV$ in the Q=10 scenario [1, 2]. At this temperature, the ITER pedestal will have electron-electron pedestal collisionality $v_e^{*ped} \lesssim 0.1$. Assessments of the ITER pedestal suggest that the limiting instabilities will be peeling modes [2] (characterized by low toroidal mode number $n \lesssim 10$), as also shown in a set of pedestal stability analysis [3] but despite the fact that this conclusion is very sensitive to the current density at the separatrix [4]. Therefore, understanding pedestal physics in low-n peeling limited plasmas and validating pedestal predictions in these conditions are essential to strengthen and improve ITER predictions.

The pedestal behaviour strongly depends on the limiting edge instability. Pedestals limited by peeling modes are expected to have an increasing pedestal pressure (p^{ped}) with increasing pedestal density (n^{ped}) and with increasing separatrix density (n^{sep}) , as observed and modelled in DIII-D [5]. Plasmas limited by balloning modes are characterized by a decreasing pedestal pressure with increasing n^{ped} [6, 7] and by a clear degradation of the pedestal performance with increasing n^{sep} [7, 8]. Since ITER will operate at high n^{ped} , high n^{sep} [9] and in mixed deuterium plasmas, assessing the role of the density and of the isotope mass in peeling limited pedestals is essential to guarantee a high ITER performance. Unfortunately, pedestals limited by peeling modes have been achieved so

far only in DIII-D [5], in some in NSTX pulses [10] and in some Alcator C-mod pulses [11]. Until recently, all other machines have not been able to reach stationary plasmas limited by peeling instabilities.

In the most recent years, a significant effort has been devoted to reach peeling limited pedestals in European machines in order to (1) understand if peeling limited pedestals can be reached in metal wall machines, (2) study pedestal physics and (3) validate pedestal predictions in ITER-relevant conditions. In JET-ILW, peeling limited pedestal have been reached by increasing q_{95} at constant I_p [12], in MAST-U via a plasma shape effect at high power [13, 14] and in TCV by operating at high power [15]. This work compares the pedestal behaviour in the peeling limited scenarios achieved in JET-ILW, MAST-U and TCV and validates the pedestal predictions in these scenarios with the predictive code Europed [16].

The work is organized as follow. Section 2 describes how peeling limited pedestals have been reached in JET-ILW, MAST-U and TCV. Sections 3 describes the effects of density scans in these scenarios and compares the results with the Europed predictions in the three machines. Section 4 presents the effect of the isotope mass, in a scan from pure deuterium to tritium-rich plasmas, in JET-ILW. Sections 5 applies Europed to the Q=10 ITER scenario to assess the type of expected pedestal instabilities. Finally, section 6 presents the conclusions.

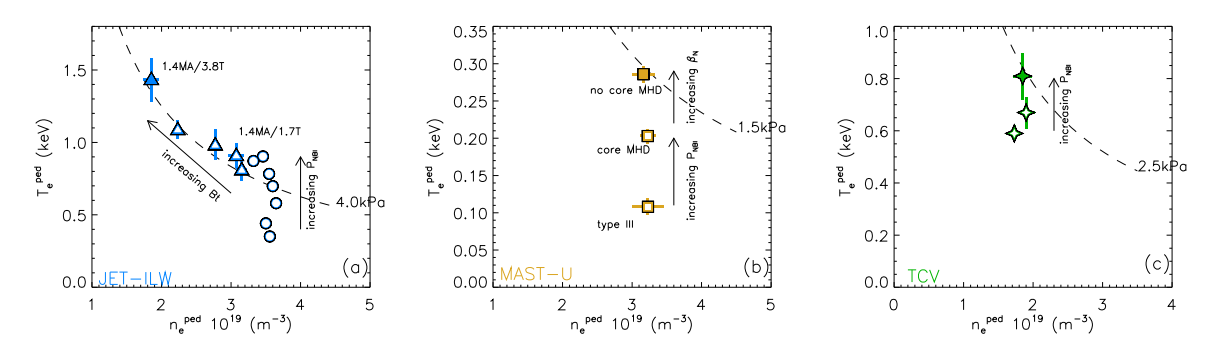


FIG. 1. Pre-ELM electron pedestal temperature versus electron pedestal density in JET-ILW (a), MAST-U (b) and TCV (c) showing how the peeling limited pedestal have been reached. The empty symbols highlight pedestals limited by ballooning modes and the full symbol the pedestal that has achieved peeling instabilities.

2. REACHING PEELING LIMITED PEDESTALS IN JET-ILW, MAST-U AND TCV

To reach peeling limited pedestals, a key condition is to achieve low collisionality. In both JET-ILW, MAST-U and TCV this has been obtained by operating with the maximum power compatible with no shine-through and reionization issues (to achieve high temperature) and at low current (to have low density). However, these conditions are not necessarily sufficient. Fig. 1(a) shows the example for JET-ILW where the circles show the effect of increasing power in a 1.4MA/1.7T high-triangularity plasma ($\langle \delta \rangle = 0.4$). Despite the increase of the electron pedestal temperature T_e^{ped} at constant electron pedestal density n_e^{ped} , the pedestal remains limited by ballooning modes and by coupled peeling-ballooning modes [17]. To achieve peeling limited pedestals it was necessary to increase the magnetic field at constant current and power ($I_p = 1.4MA, P_{NBI} = 25MW$) from $B_t = 1.7T$ to $B_t = 3.8T$, reaching $q_{95} = 8.5$. As shown by the triangles in Fig. 1(a), the increase in B_t leads to a reduction in n_e^{ped} and an increase in T_e^{ped} . The pedestal stability diagram of the pulse at the highest field (the full triangle in Fig. 1a) is shown in Fig. 2(a). The experimental pedestal has reached the peeling boundary (despite still being close to the corner) and it is limited by low-n instabilities with a dominant peeling component, as shown by the profiles of the corresponding eigenfunctions in Fig. 2(d).

Peeling limited pedestal in MAST-U have been reached by high power operation and by using an optimized plasma shape with high triangularity and high elongation [13, 14] operating at 750kA/0.5T, $q_{95} = 6.7$, $P_{NBI} = 3.2MW$, $\langle \delta \rangle = 0.5$, and $\kappa = 2.1$. While the optimized plasma shape is essential to reach peeling limited pedestals in MAST-U [13], operating at high power and high β_N is also necessary. As shown in Fig. 1(b), the increase of the power from 1.6MW to 3.2MW doubles T_e^{ped} . However, in presence of core MHD, the pedestal temperature is still around only 0.2keV and the pedestal does not reach peeling instabilities. Only in plasmas without core MHD, with $\beta_N \approx 3.0$ and $T_e^{ped} \approx 0.3keV$, peeling limited pedestals have been reached. The stability diagram of the pedestal at highest T_e^{ped} in Fig. 1(b) (the full square) is shown in Fig. 2(b). The experimental pedestal is at the peeling boundary and limited by low-n instabilities with a dominant peeling component (Fig. 2e).

Peeling limited pedestals in TCV have been achieved by operating at high power using both NBI and ECRH. The scenario has high triangularity $\langle \delta \rangle = 0.5, 155kA/1.4T, q_{95} = 5.4$ and is heated by 1.0MW via NBI and 1.1MW X2 ECRH. Fig. 1(c) shows the behaviour of T_e^{ped} and n_e^{ped} with increasing P_{NBI} but at constant P_{ECRH} . Like for JET-ILW and MAST-U the increasing P_{NBI} leads to an increase in T_e^{ped} at constant n_e^{ped} and therefore to a decrease in v_e^{*ped} . The pedestal with higher temperature (the full star in Fig. 1c) is limited by very low-n

instabilities (n = 1 - 3), as shown in Fig. 2(c). Despite the experimental point is not fully at the peeling boundary, the limiting instabilities have a strong peeling component, as shown by the eigenfunctions in Fig. 2(f).

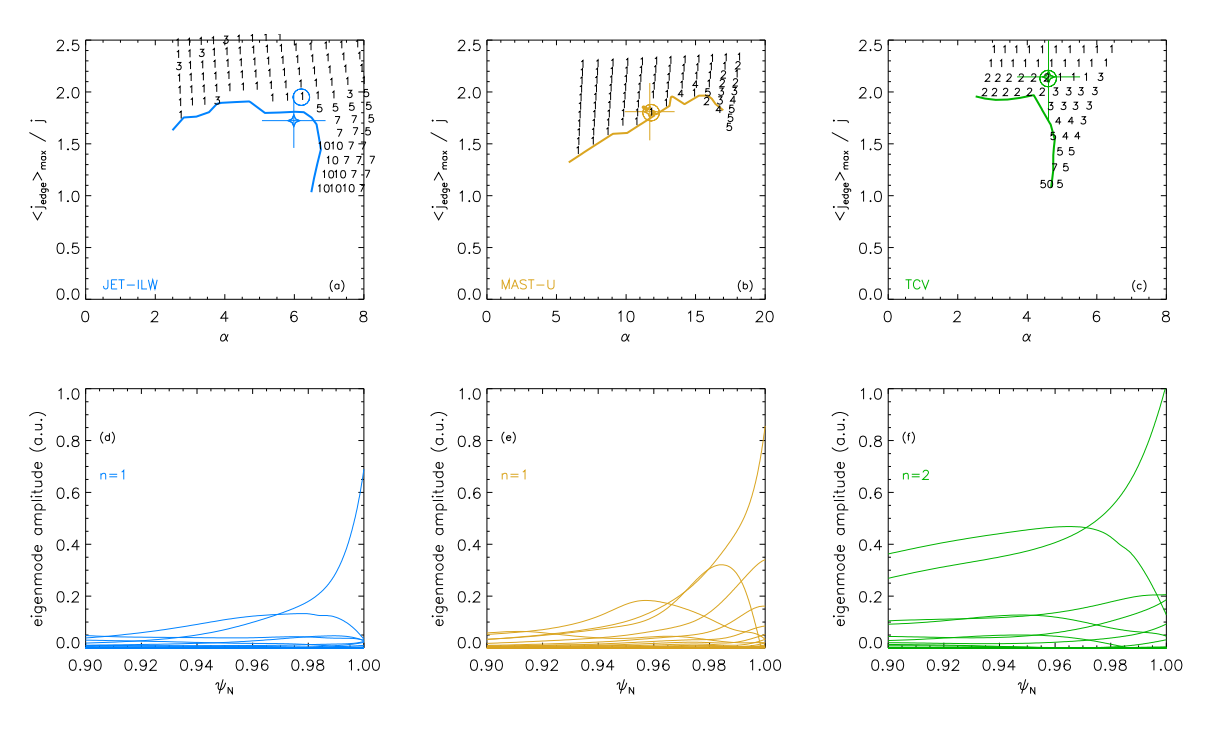


FIG. 2. Peeling ballooning stability analysis of the highest T_e^{ped} pedestals of Fig. 1 (highlighted by full symbols) for JET-ILW (a), MAST-U (b) and TCV (c). The numbers identify the toroidal mode number of the most unstable mode and the continuous line the stability boundary. The experimental pedestal with error bars is highlighted by the star. The bottom frames show the eigenfunction radial profiles of the mode highlighted by the circle in the top frames. In all the three machines, the pedestal stability analysis was done using HELENA for the equilibrium, MISHKA for the stability and using the diamagnetic criterion.

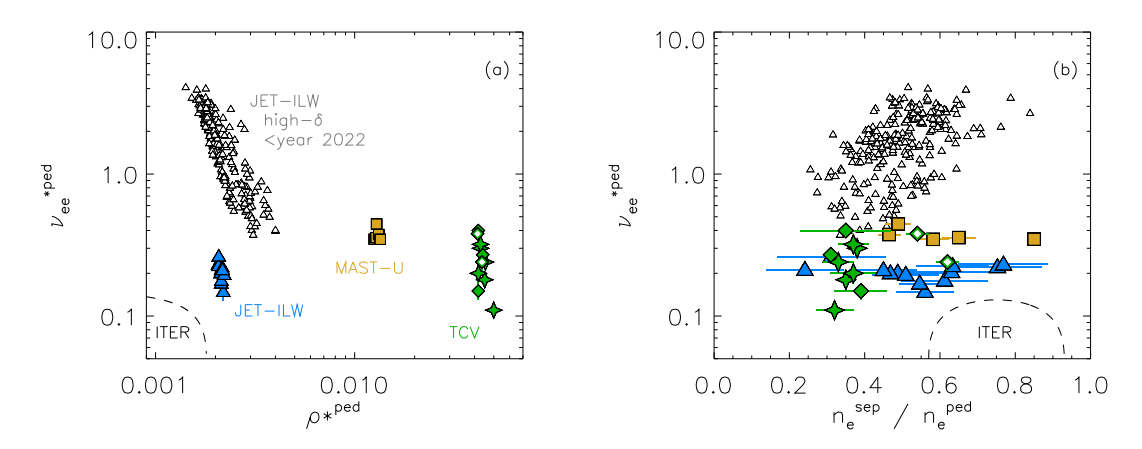


FIG. 3. Normalized dimensionless parameters space achieved via gas scans starting from the peeling limited plasmas of Fig. 1. Frame (a) shows the electron-electron pedestal collisionality versus the normalized ion Larmor radius. Frame (b) shows electron-electron pedestal collisionality versus the ratio between electron separatrix density and electron pedestal density. For comparison, the empty triangles show all the JET-ILW high triangularity plasmas achieved till 2022. All pulses have high triangularity, apart the five TCV pulses highlighted with diamonds (low triangularity). The TCV pulses highlighted with full symbols are with baffles, while those with empty symbols are without baffles.

3. EFFECT OF THE DENSITY IN PEELING LIMITED PEDESTALS IN JET-ILW, MAST-U AND TCV **3.1. The datasets**

Gas scans have been performed starting from the highest T_e^{ped} pulses of Fig. 1 (the full symbols) to vary the density in peeling limited plasmas. The variation in the gas rate has allowed to change n_e^{ped} in all the three machines. In JET-ILW, the increase of the gas rate has also increased the separatrix density n_e^{sep} , allowing for a variation in n_e^{sep}/n_e^{ped} (see details in [12]). In MAST-U, the gas rate variation has not significantly changed n_e^{sep} ,

so the achieved range in n_e^{sep}/n_e^{ped} is due only to a change in n_e^{ped} . In TCV, the increase in the gas rate has led to an increase in both n_e^{sep} and n_e^{ped} keeping n_e^{sep}/n_e^{ped} approximately constant. In TCV, to reach a variation of n_e^{sep}/n_e^{ped} , peeling limited pedestals have been compared in low triangularity pulses performed with and without baffles at otherwise identical engineering parameters. Operation with and without baffles allows different divertor neutral pressure and different neutral density and therefore a change in n_e^{sep}/n_e^{ped} [18]. An overview of relevant dimensionless parameters achieved in the three machines is shown in Fig 3. Fig. 3(a) shows v_e^{*ped} versus the normalized ion Larmor radius ρ^{*ped} . The collisionality range achieved is in the range $v_e^{*ped} = 0.1 - 0.4$ for JET-ILW and TCV (and a bit higher in MAST-U), approaching values comparable to those expected in ITER. The JET-ILW dataset has approached ρ^{*ped} comparable to ITER, while ρ^{*ped} remains significantly higher for MAST-U and TCV (due to the machine size). The datasets also reach n_e^{sep}/n_e^{ped} comparable to that of ITER, as shown in Fig. 3(b). For comparison, the grey empty triangles in Fig. 3 show all the JET-ILW high triangularity plasmas achieved till 2022. It is clear that the peeling limited JET-ILW dataset reaches dimensionless parameters much closer to ITER than any JET-ILW high- δ plasma obtained till 2022. However, as explained in section 2, to achieve these ranges, operation at very high q_{95} was necessary, well above the ITER value.

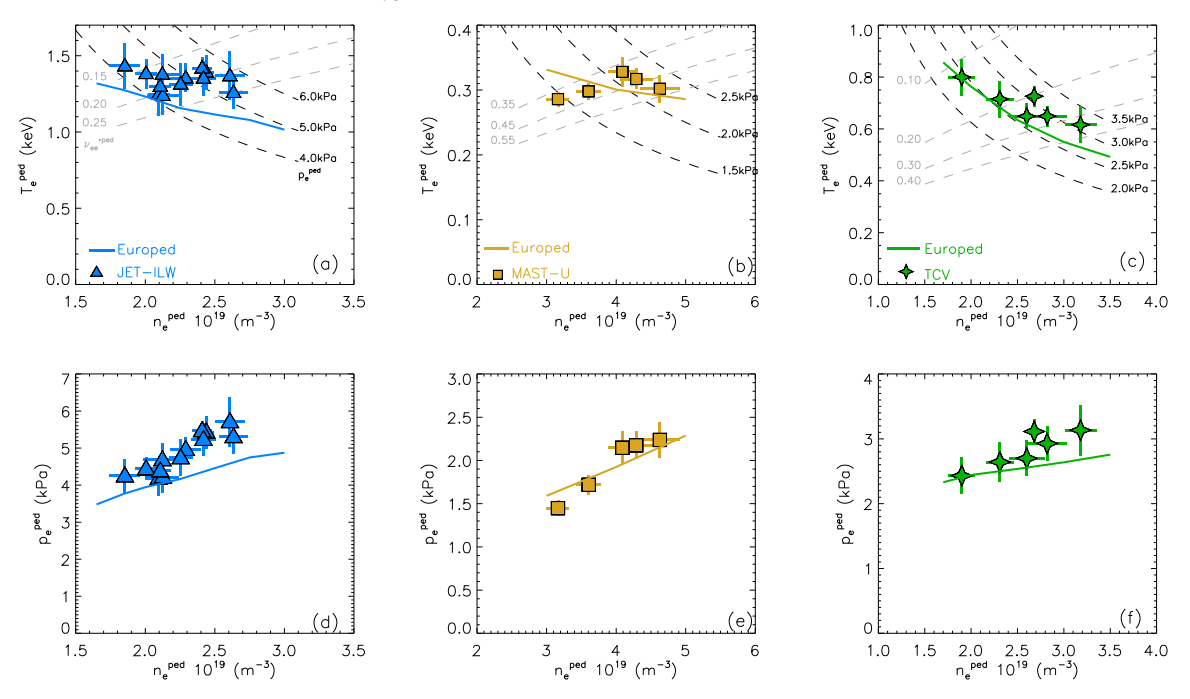


FIG. 4. Electron pedestal temperature (top frames) and electron pedestal pressure (bottom frames) versus pedestal density in JET-ILW, MAST-U and TCV. The black dashed lines in the top frames highlight the isobars while the grey dashed lines highlight the curves at constant pedestal collisionality. The continuous lines show the Europed pedestal predictions.

3.2. The effect of pedestal density

The effect of the n_e^{ped} on the pedestal height of electron temperature and pressure is shown in Fig. 4. The pedestal analysis has been carried out considering the pre-ELM profiles and assuming the separatrix temperature determined from the two-point model as described in [19]. In JET-ILW and in MAST-U, the increase of n_e^{ped} does not lead to any major variation in T_e^{ped} , while in TCV only a weak reduction can be observed. In the top frames of Fig. 4, the black dashed lines highlight the isobars at constant p_e^{ped} and the grey dashed lines highlight constant v_e^{*ped} . It is clear that the increasing n_e^{ped} leads to an increase in collisionality but also an increase in the pedestal pressure. For completeness, the bottom frames in Fig. 4 show the behaviour of p_e^{ped} with increasing density. It is important to note that this behaviour is opposite to what experimentally observed in ballooning limited pedestals, where a decreasing p_e^{ped} with increasing density is observed.

The continuous lines in Fig. 4 show the corresponding Europed predictions. For each machine, Europed has been run using the input parameters corresponding to the lowest density pulse and the simulation has been repeated by increasing n_e^{ped} while keeping all other input parameters constant $(I_p, B_t, \beta_N, n_e^{sep}/n_e^{ped})$. Qualitatively, Europed correctly predicts the increase of p_e^{ped} with increasing n_e^{ped} but quantitatively the increase is weaker than what observed experimentally.

The positive correlation between p_e^{ped} and n_e^{ped} is due to a stabilizing effect of the density on the peeling modes [12], suggesting that the increase in the pedestal pressure is mainly due to the increase of its gradient. This hypothesis is tested in Fig. 5, where the top frames show the maximum pressure gradients (∇p_e) and the bottom frames show the pressure width (w_{pe}). Indeed, in the JET-ILW dataset, ∇p_e increases with increasing n_e^{ped} while w_{pe} is constant, therefore confirming the hypothesis. In the MAST-U dataset, ∇p_e increases with increasing n_e^{ped} but also w_{pe} shows a weak increase. Therefore in MAST-U the positive correlation between p_e^{ped} and n_e^{ped} is due to both an increase in the pressure gradient (due to the stabilization of peeling modes) but also to a widening of the pressure. The TCV dataset instead show no correlation of ∇p_e with n_e^{ped} but a positive correlation between w_{pe} and n_e^{ped} . Therefore, for TCV the positive correlation between p_e^{ped} and n_e^{ped} is due only to an increase of the pressure width. The comparison with the Europed predictions in Fig. 5 are shown with continuous lines. For both the JET-ILW dataset and the MAST-U dataset, Europed predictions are in agreement with the experimental results within 10-20%. In the TCV case, the difference between predictions and experimental results is stronger and up to a factor 2. The reason between this disagreement is unclear at the moment. A possible reason might be related to a strong change in the pedestal turbulence during the density scan (which cannot be predicted in Europed), perhaps related to the fact that the TCV dataset has a significantly higher Larmor radius than the other machines (see Fig. 3).

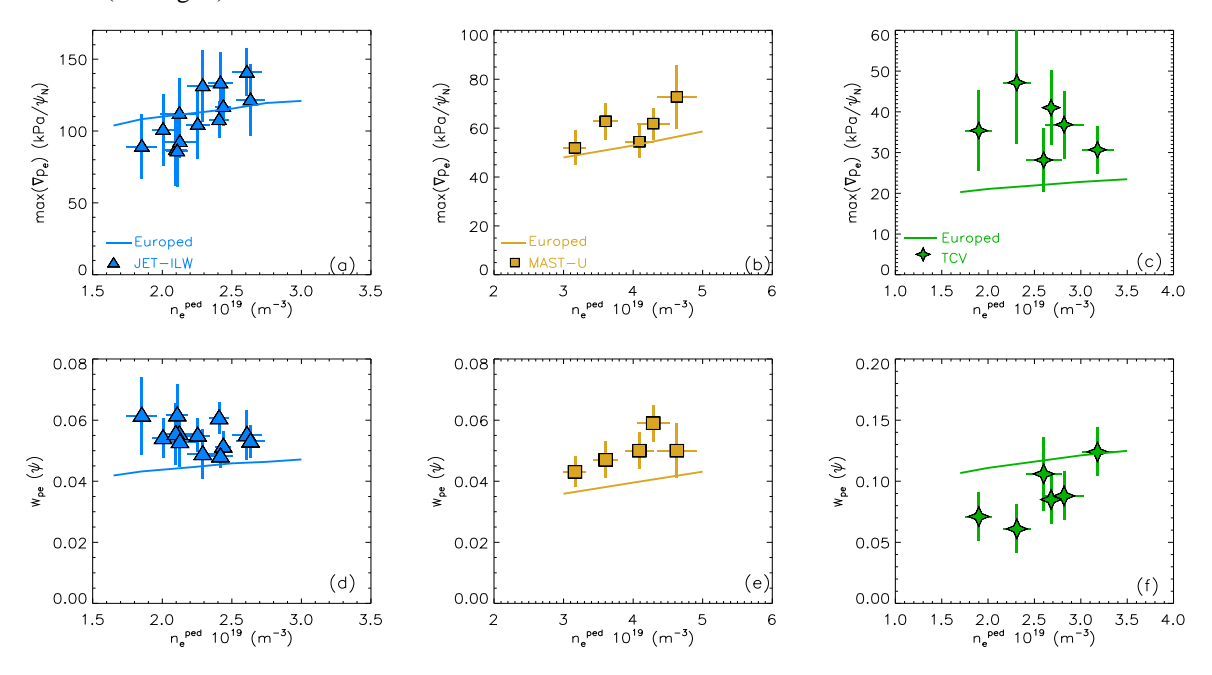


FIG. 5. Electron pedestal pressure gradients (top frames) and electron pedestal pressure width (bottom frames) versus pedestal density in JET-ILW, MAST-U and TCV. The continuous lines show the Europed pedestal predictions.

3.3. The effect of separatrix density

The effect of n_e^{sep}/n_e^{ped} on the pedestal pressure is shown in Fig. 6. Since the n_e^{ped} affects the pedestal pressure (as shown in Fig. 4), the data of Fig. 6 have been selected to have similar n_e^{ped} , so that the variation in n_e^{sep}/n_e^{ped} is due only to the separatrix density. Unfortunately, in the MAST-U dataset no major variation in n_e^{sep} has been achieved, so no MAST-U data are shown. As mentioned above, in TCV the variation in n_e^{sep} has been achieved by comparing low triangularity pulses with baffles (full diamonds) and without baffles (empty diamonds) at otherwise similar engineering parameters. In both the JET-ILW subset and the TCV subset, no correlation between p_e^{ped} and n_e^{sep}/n_e^{ped} can be observed. This is opposite to what observed in balloning limited pedestals, where a strong pedestal degradation was observed with increasing n_e^{sep}/n_e^{ped} [7,8]. The Europed predictions show a very good qualitative agreement with the experimental results, as shown by the continuous lines in Fig. 6. It is worth noting that the increase in n_e^{sep}/n_e^{ped} lead to a change in the pedestal stability. While at low n_e^{sep}/n_e^{ped} both JET-ILW and TCV were limited by low- n_e^{sep} peeling modes (see Fig. 2), the increase in n_e^{sep}/n_e^{ped} destabilizes the ballooning modes [7, 8] moving the pedestal towards the ballooning boundary. This is shown in the stability diagrams of Fig. 6, where in both machines the most unstable modes are in the range n_e^{sep}/n_e^{sep}

3.4. The effect of n_e^{ped} and n_e^{sep}/n_e^{ped} on the pedestal instability type.

The results of Fig. 6 suggest that the pedestal can transition from being limited by peeling instabilities to being limited by ballooning instabilities due the increase in n_e^{sep}/n_e^{ped} . A similar effect can be expected by the increase in n_e^{ped} at constant n_e^{sep}/n_e^{ped} , which can also lead to a destabilization of the ballooning modes. To confirm these statements, a set of Europed predictions have been performed in the three machines by first increasing n_e^{ped} at constant n_e^{sep}/n_e^{ped} and then by increasing n_e^{sep}/n_e^{ped} at constant n_e^{ped} . Fig. 7 shows the toroidal number of the critical most unstable mode. Both at low n_e^{ped} and at low n_e^{sep}/n_e^{ped} the predicted pedestal is limited by peeling modes, with $n_{crit} \leq 2$. However, in JET-ILW and in TCV the increase in n_e^{ped} and in n_e^{sep}/n_e^{ped} destabilizes higher n modes and the pedestal starts to be limited by ballooning modes or coupled peeling-ballooning modes. In MAST-U, likely because of the optimized plasma shape with high elongation, the pedestal remains firmly limited by peeling modes. Since ITER will operate at high n_e^{sep}/n_e^{ped} , the result of Fig. 7 suggests that ITER might not be limited by peeling modes despite its low collisionality. This issue is investigated in section 5.

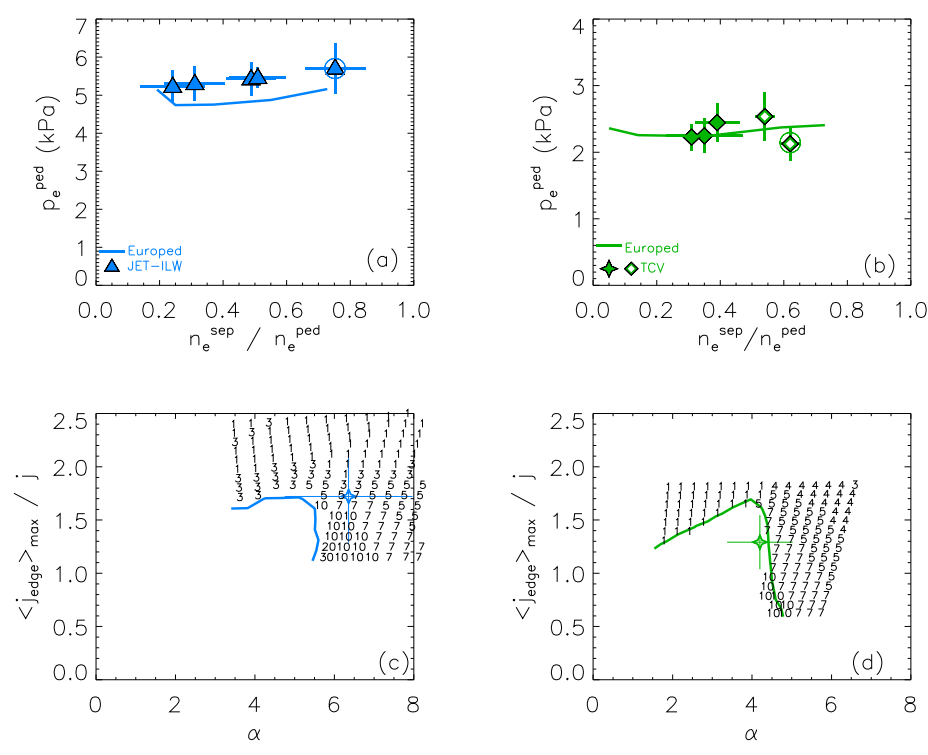


FIG. 6. The top frames show the electron pedestal pressure versus the ratio between separatrix density and pedestal density in the JET-ILW and TCV. In both machines, the data have been selected so that the variation in $n_e^{\rm sep}/n_e^{\rm ped}$ is due only to $n_e^{\rm sep}$ (i.e. constant $n_e^{\rm ped}$). The continuous line shows the Europed prediction. The bottom frames show the pedestal stability analysis for the pulses with the highest $n_e^{\rm sep}/n_e^{\rm ped}$ (highlighted by circles in the top frames).

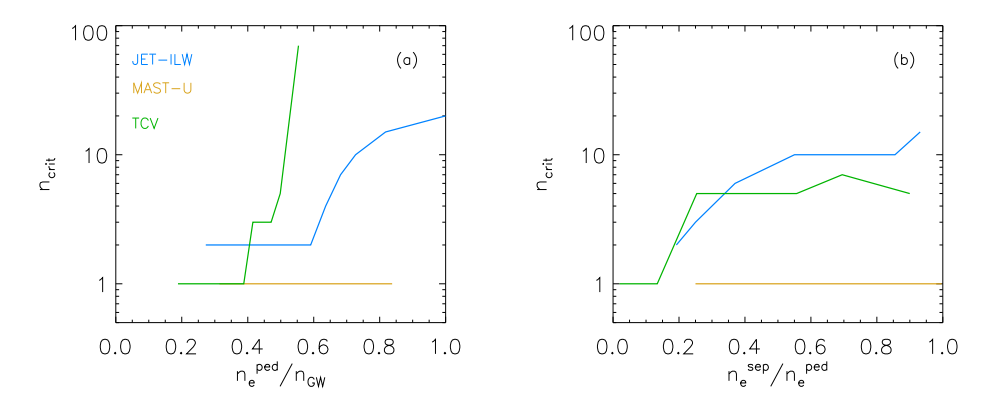


FIG. 7. Predicted most unstable mode in Europed scans of n_e^{ped} at constant $n_e^{\text{sep}}/n_e^{\text{ped}}$ (a) and $n_e^{\text{sep}}/n_e^{\text{ped}}$ at constant n_e^{ped} .

4. EFFECT OF THE ISOTOPE MASS IN PEELING LIMITED PEDESTALS IN JET-ILW

To assess the effect of the isotope mass, a gas rate scan has been performed in JET-ILW during the DTE3 campaign in tritium-rich (T-rich) plasmas (using pure tritium as main gas but deuterium in the NBI) reaching an effective mass $A_{eff}=2.9$ [12]. Apart from the isotope mass, the same engineering parameters described in section 2 have been used ($I_p=1.4MA$, $B_t=3.8T$, $P_{NBI}=25MW$, $\langle\delta\rangle=0.4$). The effect of the isotope mass on the pedestal height is show in Fig. 8. The T-rich plasmas can reach higher pedestal density than the pure deuterium plasma. Since no variation in T_e^{ped} is observed with increasing isotope mass, Fig. 8(a), the increase in n_e^{ped} leads to an increase in the pedestal pressure, as shown in Fig. 8(b). Several similarities can be seen with the higher collisionality ballooning limited plasmas obtained during the DTE2 campaign [20]. Both in the ballooning limited pedestals and in the peeling limited pedestals, the increase of the isotope mass from $A_{eff}=2.0$ to $A_{eff}=3.0$ has led to an increase in n_e^{ped} , no major variation in T_e^{ped} and an increase in p_e^{ped} . The reasons for the p_e^{ped} increase is likely related to a change in the inter-ELM particle transport, as pointed out in [20, 21]. The increase in p_e^{ped} in peeling and ballooning limited pedestal is instead due to a different effect of p_e^{ped} on the pedestal stability. In peeling limited pedestals, the increase of p_e^{ped} due to the increase in p_e^{ped} , as shown in Fig. 8(c). Indeed, the deuterium and T-rich datasets have the same trends in Fig. 8. The Europed predictions shown in Fig. 8 confirm that the higher pressure achieved in the T-rich plasma is not due to a direct effect of the isotope mass on the pedestal stability. Instead, in the ballooning limited pedestals, the increase p_e^{ped} has a destabilizing effect on the ballooning modes and the increase in the pressure is due to the direct effect of p_e^{ped} to the resistive MHD stability [12, 20].

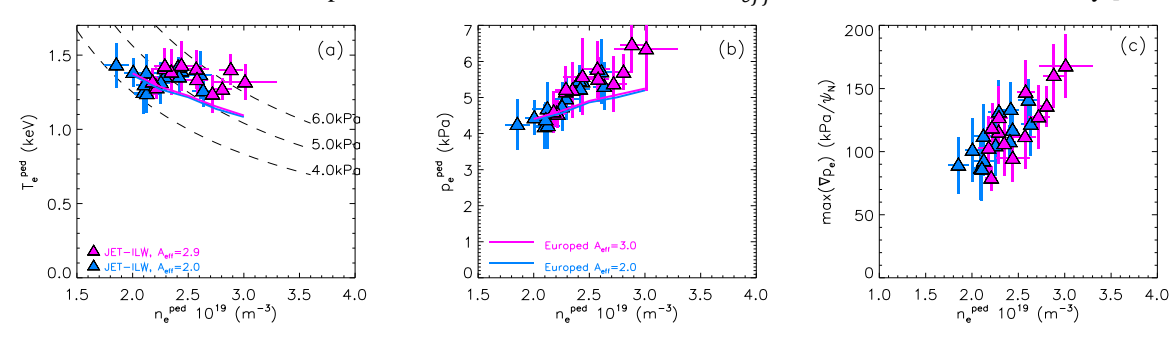


FIG. 8. Electron pedestal temperature (a), pressure (b) and maximum pressure gradient (c) versus electron pedestal density in deuterium (blue) and T-rich (magenta) plasmas in JET-ILW. The continuous lines show the Europed predictions assuming deuterium and tritium plasmas.

5. PREDICTION OF THE PEDESTAL INSTABILITIES IN THE 0=10 ITER SCENARIO

The results of the previous sections show that, from a qualitative point of view, Europed can predict reasonably well the pedestal in peeling limited plasmas, strengthening the validity of Europed for ITER predictions. This section applies Europed to predict both the type of pedestal instabilities and the pedestal pressure height in the ITER Q=10 scenario at $I_p=15MA$, $B_t=5.3T$, $\beta_N=2$ and using the plasma shape before the new ITER baseline. The main goal of the predictions has been to identify the type of pedestal instabilities that will limit ITER pedestals in type I ELMy H-modes. For this, a scan has been performed in n_e^{ped} at constant n_e^{sep}/n_e^{ped} and then repeated with different values of n_e^{sep}/n_e^{ped} . The toroidal number of the predicted most unstable mode is shown in Fig. 9(a). At low n_e^{ped} and low n_e^{sep}/n_e^{ped} , the predicted most unstable mode is in the range n=1-2, so clearly a peeling mode. At high n_e^{ped} and high n_e^{sep}/n_e^{ped} , the predicted most unstable mode is in the range n=15-20, so clearly a balloning mode or a coupled peeling-ballooning mode. The transition region from low n to high n is relatively sharp and therefore, according to the results of Fig. 9(a), the type of instability that will limit ITER pedestal might change significantly for minor changes of n_e^{ped} and n_e^{sep}/n_e^{ped} . The predictions have been extended by performing sensitivity tests in B_t and β_N . The results show that the transition region (from low n to high n) is very sensitive to B_t and less sensitive to β_N . A small increase in B_t from 5.3T to 5.4T significantly shifts the transition region to higher n_e^{ped} and higher n_e^{sep}/n_e^{ped} , while an increase in β_N from 2.0 to 2.5 only marginally shifts the transition region.

A transition to ballooning limited pedestals might be a concern for ITER, since decreasing pedestal pressure with increasing n_e^{ped} and n_e^{sep}/n_e^{ped} can be expected. However, the results of Fig. 9 suggests that this issue will not be a major problem for ITER. Examples of the predicted pedestal pressure are shown in Fig. 9(b) for n_e^{ped} =4×

 $10^{19}(m^{-3})$, dashed line, and $n_e^{ped} = 10 \times 10^{19}(m^{-3})$, continuous line. In both cases, the increasing n_e^{sep}/n_e^{ped} leads only to 6-7% reduction in p_e^{ped} . This is because the transition to high-n instabilities occurs to already relatively high n_e^{sep}/n_e^{ped} , in a region where the separatrix density has minor effect on the stability [8]. Moreover, regardless of the density, the pedestal pressure remains in the range $p_e^{ped} = 55 - 65kPa$ with no major pressure degradation observed.

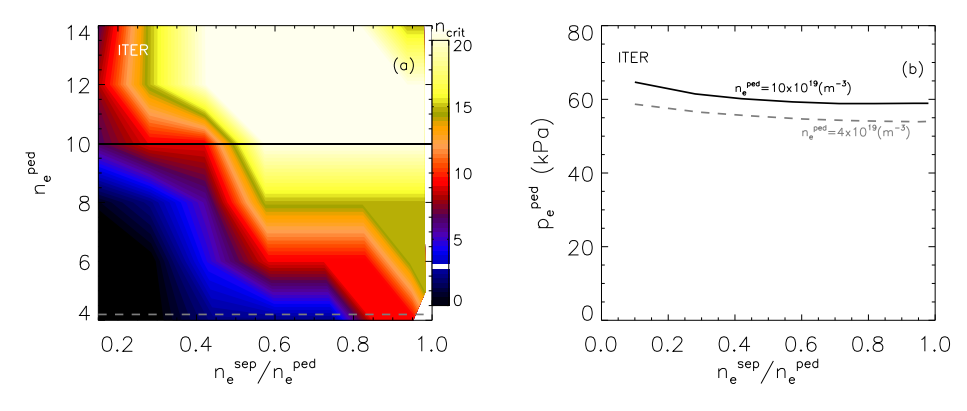


FIG. 9. Europed predictions for the Q=10 ITER scenario. Frame (a) shows the predicted toroidal number of the most unstable pedestal instability versus n_e^{ped} and n_e^{sep}/n_e^{ped} . Frame (b) shows the predicted pedestal pressure versus n_e^{sep}/n_e^{ped} at low and high pedestal density.

6. CONCLUSIONS

Pedestals limited by low-n peeling modes have been achieved in JET-ILW, MAST-U and TCV. In all the three machines, the pedestal pressure increases with increasing pedestal density and in JET-ILW and TCV, where a n_e^{sep}/n_e^{ped} scan has been achieved, no pedestal degradation has been observed with increasing n_e^{sep}/n_e^{ped} . An isotope mass scan in peeling limited JET-ILW plasmas, from pure deuterium to T-rich plasmas, has shown that increasing A_{eff} increases the pedestal pressure due to the stabilizing effect of an increased pedestal density. Moreover, Europed predictions show a reasonable qualitative agreement with the experimental results validating, at least in part, pedestal predictions in peeling limited plasmas. Finally, Europed has been applied to the Q=10 ITER scenario. The results show that ITER pedestal might be either limited by peeling or ballooning modes and that the type of instability is very sensitive to n_e^{ped} , n_e^{sep}/n_e^{ped} and B_t . Nonetheless, the results of this work are very positive for ITER. ITER will operate at high n_e^{sep}/n_e^{ped} and in mixed deuterium/tritium plasmas and this work shows that no degradation is expected by the high n_e^{sep}/n_e^{ped} operation (as instead obtained in all the ballooning limited plasma) and that a 20% increase in the pedestal pressure can be expected from the pure deuterium plasmas to the mixed deuterium/tritium plasmas.

ACKNOWLEDGEMENTS

This research is supported by Vetenskapsrådet, under grant number 2023-04895, and by Energimyndigheten under the contract number 2023-204940. This work has been carried out within the framework of the EUROfusion Consortium, partially funded by the European Union via the Euratom Research and Training Programme (Grant Agreement No 101052200-EUROfusion). The Swiss contribution to this work has been funded by the Swiss State Secretariat for Education, Research and Innovation (SERI). Views and opinions expressed are however those of the author(s) only and do not necessarily reflect those of the European Union or the European Commission or ITER. Neither the European Union nor the European Commission nor ITER can be held responsible for them.

REFERENCES

[1] Kinsey J E et al Nucl. Fusion 43 18451–54 (2003) [2] Snyder P.B. et al., Nucl. Fusion 51 103016 (2011) [3] Saarelma et al., Nucl. Fusion 52 103020 (2012) [4] P. Maget et al 2013 Nucl. Fusion 53 093011 [5] Snyder P.B. et al., Nucl. Fusion 55 083026 (2015) [6] Beurskens M. et al., Nucl. Fusion 53 013001 (2013) [7] Dunne M. et al., Plasma Phys. Control. Fusion 59, 014017 (2017) [8] Frassinetti L. et al., Nucl Fusion 61, 016001 (2021) [9] Garzotti L. et al., Nucl. Fusion 59, 026006 (2019) [10] Kleiner A et al., Nucl. Fusion 62, 076018 (2022) [11] J.W. Hughes et al 2018 Nucl. Fusion 58 112003 [12] Frassinetti L. et al., Nucl. Fusion 65, 07628 (2025) [13] K. Imada et al Nucl. Fusion 64 086002 (2024) [14] L. Frassinetti et al., 50th EPS Conf. Plasma Physics (8–12 July 2024) P1.049 [15] L. Frassinetti et al., 48th EPS Conf. Plasma Physics (27 June –1 July 2022) O4.108 [16] Saarelma S. et al., Plasma Phys. Control. Fusion 60 014042 (2018)[17] Maggi C. et al., Nucl. Fusion 55, 113031 (2015) [18] Reimerdes H. et al., Nucl. Fusion 62, 042018 (2022) [19] Silvagni d. et al., Nucl. Mat. and Energy 42, 101867 (2025) [20] Frassinetti L. et al., Nucl. Fusion 63, 112009 (2023) [21] Predebon I. et al., Nucl. Fusion 63, 036010 (2023).